INVERSION OF FULL ACOUSTIC WAVEFIELD IN LOCAL HELIOSEISMOLOGY: A STUDY WITH SYNTHETIC DATA

L. J. Cobden[1,3], C. H. Tong[2], and M. R. Warner[1]
[1] Department of Earth Science and Engineering, Imperial College London, London SW7 2AZ, UK
[2] Department of Earth and Planetary Sciences, Birkbeck, University of London, London WC1E 7HX, UK; vincent.tong@ucl.ac.uk
Received 2010 October 11; accepted 2010 November 14; published 2011 January 4

ABSTRACT

We present the first results from the inversion of full acoustic wavefield in the helioseismic context. In contrast to time–distance helioseismology, which involves analyzing the travel times of seismic waves propagating into the solar interior, wavefield tomography models both the travel times and amplitude variations present in the entire seismic record. Unlike the use of ray-based, Fresnel-zone, Born, or Rytov approximations in previous time–distance studies, this method does not require any simplifications to be made to the sensitivity kernel in the inversion. In this study, the acoustic wavefield is simulated for all iterations in the inversion. The sensitivity kernel is therefore updated while lateral variations in sound-speed structure in the model emerge during the course of the inversion. Our results demonstrate that the amplitude-based inversion approach is capable of resolving sound-speed structures defined by relatively sharp vertical and horizontal boundaries. This study therefore provides the foundation for a new type of subsurface imaging in local helioseismology that is based on the inversion of the entire seismic wavefield.

Key words: Sun: helioseismology

Online-only material: color figures

1. INTRODUCTION

Time–distance helioseismology (Duvall et al. 1993) has established itself as an important tool for imaging local solar subsurface structures in three dimensions. It relies on the measurement of the time taken for a wave packet to travel between two points on the solar surface, estimated from the cross-covariance of the observed seismic time series at the two points. The derived travel times are sensitive to the mass flows (e.g., Zhao et al. 2001; Jackiewicz et al. 2007), magnetic field (Khomenko et al. 2009), and sound-speed structure (e.g., Jensen et al. 2001) of the region which the wave traverses, and thus inversion of the travel times can be used to map the subphotospheric variations of these variables.

Early time–distance studies have used the ray approximation to forward-model and invert travel times (e.g., Giles 1999). Based on research originally developed in geophysics (e.g., Lomax & Snieder 1996; Marquering et al. 1998), several finite-frequency techniques such as Fresnel-zone, Born, and Rytov approximations have subsequently been applied to calculate the spatial sensitivity of seismic waves within the solar interior. The Fresnel-zone approximation (Jensen et al. 2000) assumes that most wave sensitivity to ambient structure lies within the first Fresnel zone, while the Born and Rytov approximations (Birch & Kosovichev 2000; Jensen & Pijpers 2003) describe the response of the wavefield to a single scatterer placed between the source and the receiver. Such approximations form the basis for inversion kernels which are significantly more realistic than those based on the ray approximation. Furthermore, studies have indicated that Fresnel-zone and Born sensitivity kernels allow solar vertical structure to be imaged at greater depths and to a higher accuracy than ray-path kernels, for the same set of travel-time data (Couvidat et al. 2004; Couvidat et al. 2006).

Over the course of the iterative inversions, ray paths change as the emerging structural variations (e.g., sound speed) deviate from the initial models, and sensitivity kernels should ideally be recalculated to reflect these changes. However, the recalculation of sensitivity kernels is computationally expensive and has not been implemented in previous helioseismic studies. Moreover, all tomographic inversions in time–distance helioseismology have hitherto been based around the fitting of the travel times of seismic waves only. By fitting both the amplitudes and timings of the wave packets, structural details can be better resolved spatially (Tong et al. 2003a), and physical parameters in the subphotosphere such as density and attenuation can be determined (Tong et al. 2003b). In the helioseismic context, Tong et al. (2003c) show, by establishing the sensitivity of the internal structure of helioseismic signals to sound-speed variations, that amplitude modeling is feasible. Such full waveform inversion has already been developed and successfully applied in terrestrial exploration seismology (e.g., Pratt et al. 1996; Chironi et al. 2006; Brenders & Pratt 2007) and studies based on cross-correlated signals from ambient terrestrial seismic noise (Shapiro et al. 2005). Wavefield inversion of cross-correlated signals from terrestrial ambient seismic noise is based on the following principle: cross-correlation of a random isotropic wavefield obtained between two points on the surface gives rise to a waveform that differs only by a factor compared with the Green function between the two points (Shapiro et al. 2005, and references therein). However, full waveform inversion has not yet been applied to helioseismic data.

In this contribution, we present results that show the first step toward applying full waveform inversion to helioseismic data (Figure 1). The aim of this study is to apply a two-dimensional full waveform inversion code to synthetic solar seismic data containing a sound-speed perturbation comparable in size and in magnitude to a sunspot. We then study the image retrieved through the inversion and discuss the implications for waveform inversion in helioseismic contexts.

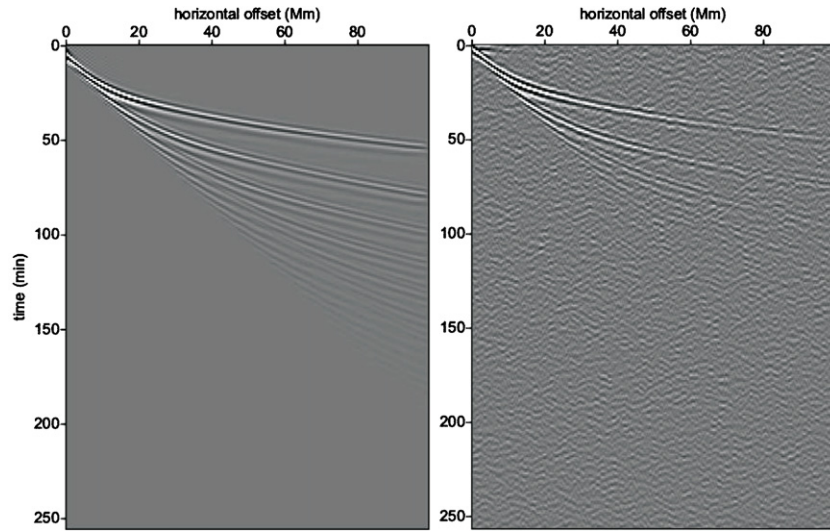[3] Current address: Department of Earth Sciences, Utrecht University, Utrecht, The Netherlands.

Figure 1. Synthetic seismic data from a single source used in this study (left panel). Cross-correlated seismic data with randomized sources (right panel). This study is based on the principle of the wavefield inversion of ambient noise that involves modeling cross-correlated signals with the Green function between the two points (Shapiro et al. 2005, and references therein).
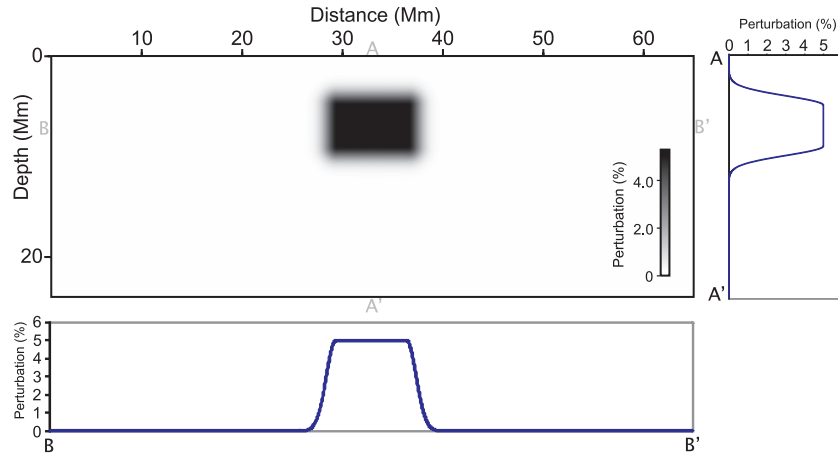

Figure 2. Sound-speed perturbation model in the wavefield tomographic study. Perturbation is expressed in terms of percentage change to the one-dimensional sound-speed structure as described by Model S (Christensen-Dalsgaard et al. 1996).
(A color version of this figure is available in the online journal.)

2. GENERATION OF SYNTHETIC DATA

We use a two-dimensional finite-difference code with a simplified acoustic wave equation (Pratt et al. 1996) to simulate the wavefield generated in a region with a sound-speed perturbation that resembles those beneath sunspots reported in previous studies (e.g., Zhao et al. 2001). The acoustic wave equation used in the code is

$$\frac{1}{\rho c^2}\frac{\partial^2 p'}{\partial t^2} = \nabla \cdot \left(\frac{1}{\rho}\nabla p'\right), \qquad (1)$$

where p' is pressure perturbation, ρ is density, and c is sound speed.

Our simulation of the seismic wavefield from one point to another on the surface in Cartesian coordinates does not involve the summation of eigenfunctions of normal modes. Unlike time–distance studies involving the use of first-order Born approximation, which only models up to the first-order terms in the perturbation (e.g., Jackiewicz et al. 2007), the code used in this study simulates the full seismic wavefield without linearizing the acoustic wave equation (Pratt et al. 1996). The perturbation is 5% faster at its maximum than the background

velocity structure, which is taken to be Model S of Christensen-Dalsgaard et al. (1996), and tapers off to background levels toward its edges with a Gaussian decay (Figure 2). We choose a perturbation with a size of the order of a few wavelengths at its upper surface, i.e., near the resolution limits of travel-time tomography, whose maximum depth is sampled by waves traversing horizontal distances contained within the width of the model. In order to study the velocity structure uniquely, the density and attenuation structures are kept laterally constant, but vary with depth according to Model S (Christensen-Dalsgaard et al. 1996) and an empirical exponential decay (Tong et al. 2003b), respectively.

Our data (Figure 1) are generated using a 1600×600 node grid, with a node spacing of 0.04 Mm. The grid has absorbing boundaries at its sides and base, and a reflecting boundary at its top surface to represent the solar photosphere. We place acoustic sources every 0.16 Mm along the model, each at a depth of 80 km below the surface, giving a total of 400 sources. The sources are impulsive, with a dominant frequency of 3.2 mHz. The use of impulsive sources placed at a constant shallow depth is consistent with observational constraints (e.g.,
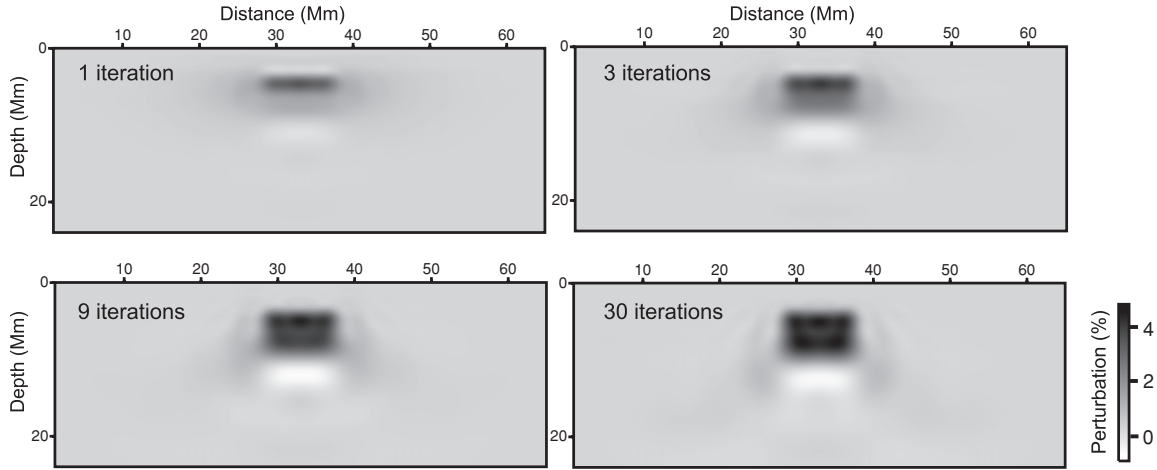
Figure 3. Recovered sound-speed structures from wavefield inversion after 1, 3, 9, and 30 iterations.

Nigam & Kosovichev 1999) and has been validated in earlier studies (e.g., Tong et al. 2003b; Shelyag et al. 2006; Parchevsky & Kosovichev 2007; Parchevsky et al. 2008; Cobden et al. 2010). The acoustic sources are not randomized in space or time, as is the case in the real Sun. This means that during inversion we are attempting to retrieve only the acoustic wavefield structure, and for the purpose of demonstrating waveform inversion in this study we have assumed that acoustic source function remains constant. Although stochastic sources have been simulated in previous helioseismic studies (Hanasoge et al. 2006; Cameron et al. 2008), our adoption of a constant acoustic source function is consistent with the approach used in current studies for constructing helioseismic forward models (e.g., Werne et al. 2004; Hanasoge et al. 2007). However, in principle it is possible to invert for the source function and wavefield structure simultaneously.

Acoustic receivers are positioned every 0.16 Mm near the top of the model. Each receiver records the pressure perturbation on the surface in response to the underlying wavefield which is calculated and recorded at intervals of 0.45 minutes (27 s) for 115 minutes. The seismic traces at each receiver are then used as input ("observed data") for the following waveform inversion.

3. INVERSION PROCEDURE

The inversion code we use is an extension of the finite-difference code used for generating the synthetic data, and hence it is built around solving a simplified wave equation in the frequency domain at the node points of a two-dimensional grid. The detailed mathematical theory behind the inversion procedure can be found in Pratt (1999). Here we present an outline of the theory.

The system for which the inversion is calculated can be represented by

$$\mathbf{u}(\omega) = \mathbf{S}^{-1}(\omega)\mathbf{f}(\omega), \qquad (2)$$

where $\mathbf{u}$, an $m \times 1$ matrix, is the Fourier-transformed, complex-valued, discretized wavefield, sampled at m node points, $\mathbf{S}$ is an $m \times m$ complex-valued impedance matrix, and $\mathbf{f}$ is an $m \times 1$ acoustic source term matrix. Note that the impedance matrix (Marfurt 1984) is a very large and sparse matrix that links the seismic source terms to the seismic wavefield (Pratt 1999).

We estimate the unknown physical properties (sound speed in our case) at the node points using

1. m sets of Fourier-transformed experimental observations, $\mathbf{u}_d$, recorded at a subset of the nodal points corresponding to the receiver locations,
2. an initial model from which synthetic data $\mathbf{u}_s$ are generated.

The inversion proceeds by iteration, for a finite (specified) number of frequencies (ω). At each iteration the sound speed structure and associated wavefield are updated. We seek to minimize the data misfit function defined by the sum of squared residual errors, $0.5\delta\mathbf{u}^T\delta\mathbf{u}^*$, where $\delta\mathbf{u} = \mathbf{u}_s - \mathbf{u}_d$. The model is updated by calculating the gradient direction of the data misfit function. Details of the computation of the gradient direction can be found in Pratt (1999).

In our particular case, the initial synthetic wavefield $\mathbf{u}_{s0}$ is computed based on the one-dimensional sound-speed profile of Model S (i.e., no sound-speed perturbations), and the data are modeled at five frequencies: 1, 1.7, 2.4, 3.1, and 3.8 mHz. These frequencies are chosen to avoid aliasing artifacts related to the model parameterization. These frequencies are selected to be consistent with observations of the power spectrum of solar oscillations (e.g., Duvall et al. 1993), which peak at 3.2 mHz. Since we have specified the source function $\mathbf{f}(\omega)$ as it is required to generate the synthetic data, it is the impedance matrix $\mathbf{S}$ which changes during inversion.

4. RESULTS

Figures 3 and 4 show the results of the waveform inversion. With an increasing number of iterations of the algorithm, the inversion scheme is capable of imaging structures with a length scale of the order of the signal wavelength (Figures 3 and 4). We note that the inversion recovers the relatively sharp vertical boundaries that are notoriously difficult to recover by travel-time-based methods. The sound speeds immediately inside and outside of the perturbation are estimated accurately. Moreover, the code is also able to map the dimensions and magnitude of the upper boundary of the perturbation in the first few iterations of the inversion.

Similar to the results reported in previous wavefield studies (e.g., Pratt 1999), the code images the lower boundary of the perturbation with more difficulty. This is partly because the seismic wavelength increases with depth, which decreases the sharpness of the lower boundary. Another reason is that the acoustic waves have to travel through the perturbation itself in order to sample its bottom edge, and therefore the code has to
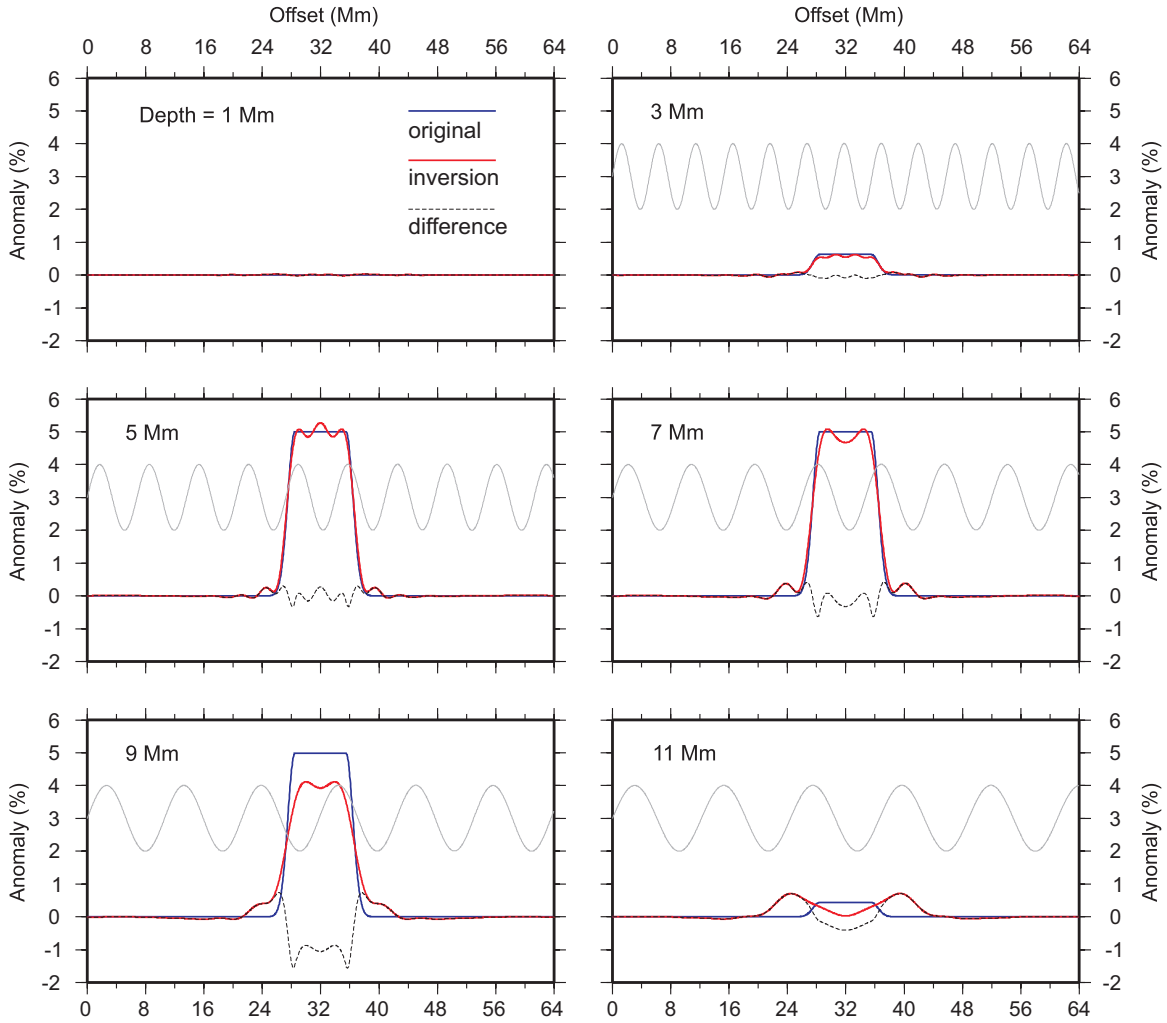
Figure 4. Recovered and original sound-speed structures at depths = 1, 3, 5, 7, 9, and 11 Mm. The differences between the recovered and original structures, and the wavelengths of p1-modes (P-waves in geophysics) at a peak frequency of 3.2 mHz (gray lines) are also shown for reference.

(A color version of this figure is available in the online journal.)

deconvolve the combined effects of the overlying sound-speed perturbation and sound-speed gradient across the boundary. In practice, this means that in the early stages of the inversion, the code underestimates the magnitude of the positive anomaly, but compensates by placing a negative anomaly immediately below it, to create the correct velocity gradient. Similar effects occur along the side edges of the anomaly with increasing depth. Note that in our code that is based on simulating acoustic waves in the Cartesian coordinate system, no explicit modeling of modes is performed (Section 2). However, the imaging problem near the bottom of our model discussed here is similar to that caused by the limitation of a finite mode set in helioseismic modeling.

5. DISCUSSION AND CONCLUSIONS

We have demonstrated in this study that full acoustic wave-field inversion can be applied to imaging sound-speed perturbations in the helioseismic context (Figures 3 and 4). In particular, the locations and magnitude of the relatively sharp vertical and horizontal boundaries at shallow depths (less than 10 Mm) can be imaged to high accuracy. The observed oscillatory artifacts near vertical boundaries (Figures 3 and 4) are intrinsically linked to frequency-based wavefield inversions and are of significantly lower amplitude than the local sound-speed perturbations. Note

that the relatively smooth models obtained from travel-time-based methods (including time–distance helioseismology) are likely to be the result of smoothing and relatively sparse model parameterization, which do not allow an accurate determination of any potentially abrupt structural changes. Our results are therefore compatible with the observations made in terrestrial seismology that full waveform inversions produce better-resolved and more realistic images than travel-time tomography (e.g., Chironi et al. 2006).

It is interesting to compare the use of wavefield approximation kernels with the full-wavefield tomographic approach. Although the Fresnel-zone, Born, and Rytov approximations implemented to simulate wave effects in previous helioseismic studies (e.g., Gizon & Birch 2002; Jensen & Pijpers 2003) involve less computational effort than full wavefield inversion, this is mainly because their sensitivity kernels were fixed throughout the inversion. Moreover, computational cost with these approximations is relatively low only if sensitivity kernels are based on the initial one-dimensional (depth-dependent-only) models. In this case, travel times are then dependent on the distance between the two points on the surface only and do not vary laterally. In other words, the approximated seismic wavefield does not take into account the deviation of structures from the initial one-dimensional starting model that occurs during the

course of inversion. If the sensitivity kernel is updated after each step in the iterative inversion, the computational cost using these approximations will increase substantially and will become comparable to full wavefield tomography, which has the advantage of higher accuracy in capturing the sensitivity of sound-speed perturbation.

The inversion of synthetic data reported in this study was performed on a single-core Xeon processor with a clock speed of 2 GHz, and the time required for performing 30 iterations with our model and synthetic dataset in this study was approximately two weeks. The computational time required for wavefield tomography is relatively high, but it is not prohibitively so given the continuous improvement in computational power and availability of multiple-core processors in desktop computers. In fact, the relatively high computational cost of wavefield tomography is not only compensated by the improvement in model resolution but also by its ability to determine the variations of other physical parameters such as attenuation and density (Tong et al. 2003b). An additional advantage of inverting the entire seismic record (i.e., amplitudes and travel times) in wavefield tomography is that the "first bounce" and the "multiple bounces" (seismic waves that have been reflected near the photosphere before reaching the receiver) can be simultaneously analyzed. Such simultaneous modeling of amplitudes and travel times will provide more constraints on structural variations such as attenuation in the solar subphotoshere.

The results presented in this study are based on the inversion of noise-free synthetic helioseismic data for sound-speed variations. Research efforts have been made to address the estimation of noise levels of data in time–distance helioseismology (e.g., Gizon & Birch 2004) and future applications of geophysical wavefield techniques to helioseismic data (Tong 2005) will need to take this into consideration. The inversion of real helioseismic data will then be able to confirm the expected improvement in model resolution with wavefield inversion as demonstrated in previous geophysical studies (e.g., Pratt 1999; Chironi et al. 2006). In our inversion, we assume that the acoustic source functions are constant. However, variations in solar source density have been shown to influence the amplitude of the helioseismic signals (Cobden et al. 2010). Further developments will be needed to apply wavefield tomography to real helioseismic data, including the use of equations that capture the physics of the magnetic field (Khomenko et al. 2009). In conclusion, our study highlights the importance of further development in the inversion of helioseismic data as most recent research efforts in local helioseismic methods tend to focus on forward modeling techniques. To this end, amplitude-based inversion methods such as wavefield tomography offer a promising avenue for better utilization of available seismic data.

REFERENCES

Birch, A. C., & Kosovichev, A. G. 2000, Sol. Phys., 192, 193
Brenders, A. J., & Pratt, R. G. 2007, Geophys. J. Int., 168, 133
Cameron, R., Gizon, L., & Duvall, T. L., Jr. 2008, Sol. Phys., 251, 291
Chironi, C., Morgan, J. V., & Warner, M. R. 2006, J. Geophys. Res., 111, B05313
Christensen-Dalsgaard, J., et al. 1996, Science, 272, 1286
Cobden, L. J., Tong, C. H., & Warner, M. R. 2010, ApJ, 725, 313
Couvidat, S., Birch, A. C., & Kosovichev, A. G. 2006, ApJ, 640, 516
Couvidat, S., Birch, A. C., Kosovichev, A. G., & Zhao, J. 2004, ApJ, 607, 554
Duvall, T. L., Jefferies, S. M., Harvey, J. W., & Pomerantz, M. A. 1993, Nature, 362, 430
Giles, P. 1999, PhD thesis, Stanford Univ.
Gizon, L., & Birch, A. C. 2002, ApJ, 571, 966
Gizon, L., & Birch, A. C. 2004, ApJ, 614, 472
Hanasoge, S. M., Duvall, T. L., & Couvidat, S. 2007, ApJ, 664, 1234
Hanasoge, S. M., Larsen, R. M., Derosa, M. L., Hurlburt, N. E., Schou, J., Roth, M., Christensen-Dalsgaard, J., & Lele, S. K. 2006, ApJ, 648, 1268
Jackiewicz, J., Gizon, L., Birch, A. C., & Duvall, T. L. 2007, ApJ, 671, 1051
Jensen, J. M., Duvall, T. L., Jacobsen, B. H., & Christensen-Dalsgaard, J. 2001, ApJ, 553, L193
Jensen, J. M., Jacobsen, B. H., & Christensen-Dalsgaard, J. 2000, Sol. Phys., 192, 231
Jensen, J. M., & Pijpers, F. P. 2003, A&A, 412, 257
Khomenko, E., Kosovichev, A., Collados, M., Parchevsky, K., & Olshevsky, V. 2009, ApJ, 694, 411
Lomax, A., & Snieder, R. 1996, Geophys. J. Int., 126, 369
Marfurt, K. J. 1984, Geophysics, 49, 533
Marquering, H., Nolet, G., & Dahlen, F. A. 1998, Geophys. J. Int., 132, 521
Nigam, R., & Kosovichev, A. G. 1999, ApJ, 514, L53
Parchevsky, K. V., & Kosovichev, A. G. 2007, ApJ, 666, L53
Parchevsky, K. V., Zhao, J., & Kosovichev, A. G. 2008, ApJ, 678, 1498
Pratt, R. G. 1999, Geophysics, 64, 888
Pratt, R. G., Song, Z.-M., Williamson, P. R., & Warner, M. R. 1996, Geophys. J. Int., 124, 323
Shelyag, S., Erdélyi, R., & Thompson, M. J. 2006, ApJ, 651, 576
Shapiro, N. M., Campillo, M., Stehly, L., & Ritzwoller, M. H. 2005, Science, 307, 1615
Tong, C. H. 2005, Phil. Trans. R. Soc., 363, 2761
Tong, C. H., Thompson, M. J., Warner, M. R., & Pain, C. C. 2003a, ApJ, 596, L263
Tong, C. H., Thompson, M. J., Warner, M. R., & Pain, C. C. 2003b, ApJ, 593, 1242
Tong, C. H., Thompson, M. J., Warner, M. R., Rajaguru, S. P., & Pain, C. C. 2003c, ApJ, 582, L121
Werne, J., Birch, A., & Julien, K. 2004, in Proc. SOHO 14/GONG 2004 Workshop, Helio- and Asteroseismology: Towards a Golden Future, ed. D. Danesy (ESA SP-559; Noordwijk: ESA), 172
Zhao, J. W., Kosovichev, A. G., & Duvall, T. L. 2001, ApJ, 557, 384